Gradients of phosphatidylserine contribute to plasma membrane charge localization and cell polarity in fission yeast

Armin Haupt* and Nicolas Minc
Institut Jacques Monod, 75205 Paris Cedex 13, France

ABSTRACT **Surface charges at the inner leaflet of the plasma membrane may contribute to regulate the surface recruitment of key signaling factors. Phosphatidylserine (PS) is an abundant charged lipid that may regulate charge distribution in different cell types. Here we characterize the subcellular distribution and function of PS in the rod-shaped, polarized fission yeast. We find that PS preferably accumulates at cell tips and defines a gradient of negative charges along the cell surface. This polarization depends on actin-mediated endocytosis and contributes to the subcellular partitioning of charged polarity-regulating Rho GTPases like Rho1 or Cdc42 in a protein charge–dependent manner. Cells depleted of PS have altered cell dimensions and fail to properly regulate growth from the second end, suggesting a role for PS and membrane charge in polarized cell growth.**

Monitoring Editor
Patricia Bassereau
Institut Curie

Received: Jun 2, 2016
Revised: Nov 7, 2016
Accepted: Nov 8, 2016

INTRODUCTION

Lipids are abundant components of biological membranes that are distributed asymmetrically within cells and can form laterally segregated domains (van Meer *et al.*, 2008; Spira *et al.*, 2012). In the case of anionic lipids like phosphatidylserine (PS), phosphatidylinositol phosphates (PIPs), and phosphatidic acid (PA), this asymmetry may give rise to differently charged domains on the cytosolic face of membranes with strong affinity for cationic species like ions (e.g., Ca^{2+}) or proteins (Olivotto *et al.*, 1996). Consequently, membrane charges have been suggested to contribute to protein localization and activity via polybasic sequence regions (Heo *et al.*, 2006; Yeung *et al.*, 2008; Li *et al.*, 2014).

PS is a minor lipid comprising 2–10% of total lipids and is especially enriched in the cytosolic leaflet of the plasma membrane (>20% of membrane lipids in yeast) (van Meer *et al.*, 2008). PS is synthesized in the endoplasmic reticulum (ER) and transits to the cell surface through the secretory pathway or directly via ER–plasma membrane contact sites (Fairn *et al.*, 2011b; Maeda *et al.*, 2013). In mammals, PS is thought to be involved in intracellular signaling via c-Raf1 or protein kinase C, endocytosis, or phagocytosis. Also, PS can be externalized on the plasma membrane under specific conditions like apoptosis or blood clotting (Nishizuka, 1992; Ghosh *et al.*, 1994; Vance, 2008; Yeung *et al.*, 2008, 2009).

In addition to its global implication in protein recruitment at the plasma membrane, PS, may also be involved in regulating cell polarity. In budding yeast, recent work using a genetically encoded probe for PS showed a systematic enrichment of this lipid at sites of polarized growth during budding and mating. A mutant strain in the PS synthase (*cho1*Δ) exhibited major polarization defects with impaired enrichment of the Rho GTPase Cdc42p (Fairn *et al.*, 2011a). A second study in the same system suggested that the dynamic exchange of PS against a neutral exoplasmic lipid, phosphatidylethanolamine, is important for Cdc42p recycling by the guanine nucleotide dissociation inhibitor Rdi1. Mutants of a flippase complex (Lem3 and Dnf1 or Dnf2) had higher PS levels at bud sites and wider Cdc42p caps, suggesting that local reduction of charges may be required for lowering the affinity of Cdc42p to the membrane (Das *et al.*, 2012). To date, however, the specific contribution of PS electrostatics to cell polarity remains understudied.

The fission yeast *Schizosaccharomyces pombe* is a well-established tractable system to study the contribution of membrane lipid domains to cell polarity and morphogenesis (Wachtler *et al.*, 2003; Chang and Martin, 2009; Makushok *et al.*, 2016). These rod-shaped

This article was published online ahead of print in MBoC in Press (http://www.molbiolcell.org/cgi/doi/10.1091/mbc.E16-06-0353) on November 16, 2016.

*Address correspondence to: Armin Haupt (armin.haupt@ijm.fr).

Abbreviations used: ANOVA, analysis of variance; DMSO, dimethyl sulfoxide; ER, endoplasmic reticulum; GFP, green fluorescent protein; LatA, latrunculin A; MBC, methyl-2-benzimidazol-2-yl-carbamate; ME, malt extract; NETO, new end take-off; ORF, open reading frame; PA, phosphatidic acid; PIP, phosphatidylinositol phosphate; PIP_2, phosphatidylinositol-4,5-bisphosphate; PS, phosphatidylserine.

Supplemental Material can be found at:
http://www.molbiolcell.org/content/suppl/2016/11/14/mbc.E16-06-0353v1.DC1.html

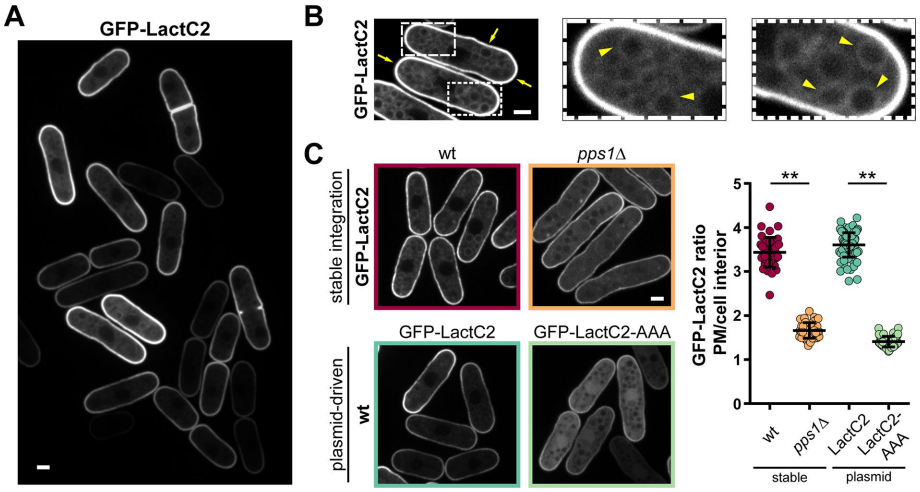

FIGURE 1: Expression of a probe for PS in fission yeast. (A) Distribution of GFP-LactC2 expressed from an inducible pREP3X plasmid in wild-type cells grown in EMM without thiamine for 48 h. (B) Subcellular localization of GFP-LactC2. Arrows point to the plasma membrane and arrowheads to intracellular membranes labeled with GFP-LactC2. Cells were grown as in A. (C) Specificity of GFP-LactC2 as a PS probe in *S. pombe*. Left, top, GFP-LactC2 stably expressed from the shk1 promotor in wild-type (wt) and *pps1*Δ cells grown in YE5S for 18 h. Bottom, left, GFP-LactC2 and GFP-LactC2-AAA expressed from the pREP3X plasmid in the wild type, grown in EMM without thiamine for 48 h. Right, quantification of signal enrichment at the plasma membrane over the cell interior (wild type $n = 41$, *pps1*Δ $n = 43$, GFPLactC2 $n = 94$, GFP-LactC2-AAA $n = 62$). Two-tailed, unpaired *t* test: **, $p < 0.0001$. Scale bars: 2 μm. All quantifications are based on at least two independent experiments. Graphs display the mean; error bars represent SDs.

cells grow at cell tips and transit from monopolar to bipolar growth during G_2 phase in a process called new end take-off (NETO). NETO involves the proper relocalization of polarity-regulating Rho GTPases such as Rho1 and Cdc42 to the new end, which involves upstream regulators such as microtubules, Tea1, and Tea4 (Chang and Martin, 2009; Perez and Rincon, 2010). In fission yeast, sterol-rich domains accumulate at growing tips and sites of cytokinesis and have been proposed to influence polarized behavior (Wachtler *et al.*, 2003; Makushok *et al.*, 2016). However, the subcellular distribution of PS and its detailed contribution to cell polarity remains largely unknown. Deletion of the single PS synthase (*pps1*Δ) has been shown to affect cell morphology, cytokinesis, and cell wall assembly. However, these defects were attributed to the lack of the PS metabolite phosphatidylethanolamine (Matsuo *et al.*, 2007).

Here we use fluorescent probes to monitor the transcellular distribution of PS and membrane charges in fission yeast. We find that PS and negative charges accumulate at cell tips and sites of cell division and that this polarized distribution depends on actin-based endocytosis. Detailed characterization of a PS synthase mutant reveals defects in membrane charge, Cdc42 and Rho1 membrane recruitment, and NETO. Thus these data suggest how membrane electrostatics may influence charged protein recruitment and consequent cell polarization.

RESULTS

PS is polarized to sites of cell growth and division

Recently, a probe for phosphatidylserine, called LactC2, has enabled the investigation of the localization of this lipid in living cells. This probe utilizes the C2 domain of bovine lactadherin (LactC2), a glycoprotein of milk that binds PS in a calcium-independent manner (Yeung *et al.*, 2008). To monitor PS localization in the fission yeast *S. pombe*, we generated two green fluorescent protein (GFP)-LactC2 expression constructs. The first one, designed for inducible expression, is cloned into the pREP3X plasmid, which contains the thiamine-repressible nmt1 promoter for strong overexpression (Maundrell, 1993). The second construct for constitutive expression is stably integrated into the genome under the control of the shk1 promoter. Both constructs revealed that GFP-LactC2 was membrane bound and preferentially localized to the plasma membrane and less abundantly to endomembranes (Figure 1, A and B, and Supplemental Figure S1, A and B). Cells expressing these constructs did not exhibit any notable defect in cell shape, dimensions, and growth rate, apart from pREP3X-driven expression that resulted in slightly longer cells at division (Supplemental Figure S1, D–G). To test the specificity of GFP-LactC2 to PS lipids, we expressed GFP-LactC2 in a PS-synthase mutant (*pps1*Δ). We detected a strong drop of global membrane labeling and plasma membrane enrichment accompanied by the emergence of cytoplasmic and nuclear signals (Figure 1C). Importantly, this loss of membrane localization was similar to that of a LactC2 mutant (LactC2-AAA), which is unable to bind PS (Figure 1C; Yeung *et al.*, 2008). We did, however, detect some residual membrane binding under these conditions, indicating some minor level of nonspecificity of the probe (Figure 1C and Supplemental Figure S1C). Taken together, these data indicate that the GFP-LactC2 probe is functional in *S. pombe* and reflects PS distribution as in other cell types (Yeung *et al.*, 2008; Fairn *et al.*, 2011b).

We next investigated PS distribution along the plasma membrane (Fairn *et al.*, 2011a). Strikingly, in wild-type cells, GFP-LactC2 was enriched at both cell tips and formed a gradient that slowly subsided from the edge of the tip to the cell sides (Figures 1A and 2, A and B). The ratio of tip to side signal showed a tip enrichment of ~1.6-fold. In contrast, GFP-PH, a probe for another charged lipid, phosphatidylinositol-4,5-bisphosphate (PIP_2), did not show such significant accumulation (tip:side ratio ~1.1), indicating that this tip accumulation was PS specific (Figure 2B; Zhang *et al.*, 2000). Monitoring GFP-LactC2 distribution over the cell cycle showed that, during interphase, high PS levels are continuously present at both cell tips and that PS relocalizes to the center of the cell during mitosis and cytokinesis (Figure 2C and Supplemental Movie S1). Calcofluor staining, which labels sites of cell wall synthesis, confirmed that PS is enriched at sites of cell growth and septum assembly (Supplemental Figure S2A). Close inspection of cells from an unsynchronized culture further revealed that GFP-LactC2 concentrates at future sites of cytokinesis before membrane ingression and is most enriched in regions close to the constricting ring (Figure 2D). Measurements of GFP-LactC2 intensities revealed an enrichment of ~twofold in cytokinetic membranes compared with lateral membranes (Figure 2E). Following cell separation, GFP-LactC2 intensity remained high at new cell ends, even in the absence of growth (Figure 1A and Supplemental Figure S2B). Comparison of both cell ends showed that the intensity at new ends was slightly higher than at old ends in short cells and decreased through the course of interphase to reach similar levels as at the old tip when cells reached a length of

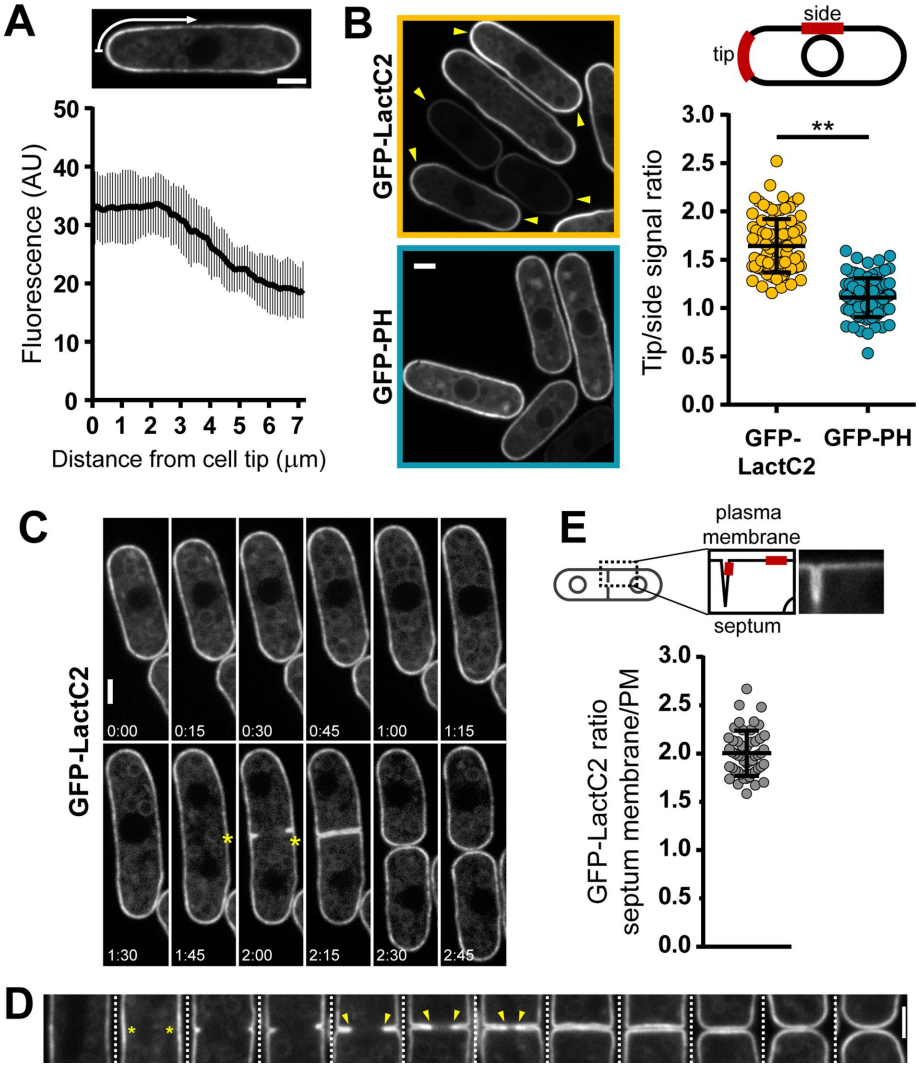

FIGURE 2: PS is polarized in vegetative fission yeast cells. (A) Tip enrichment of shk1-GFP-LactC2 in wild-type cells. Top, cell with an indication of how the fluorescence gradient is measured around the contour. Bottom, average GFP-LactC2 gradient emanating from cell tips ($n = 39$). (B) Comparison of cell tip enrichment of probes detecting PS (pREP3X GFP-LactC2, yellow) and PIP_2 (pREP1 GFP-PH, cyan). Left, fluorescence images of both probes. Arrowheads point to interphase cell ends enriched in the respective probe. Right, top, schematic of measurements of tip:side ratios at the plasma membrane. Right, bottom, quantification of tip:side ratios (pREP3X GFP-LactC2 $n = 94$, pREP1 GFP-PH $n = 84$). Two-tailed, unpaired t test: **, $p < 0.0001$. Expression of GFP-PH was induced for 16 h at 30°C. (C) Cell cycle–dependent distribution of shk1-GFP-LactC2. Asterisks point at sites of PS enrichment at the cell center during cytokinesis. Elapsed time is in h:min. (D) GFP-LactC2 is polarized during cytokinesis. Different cells expressing GFP-LactC2 from pREP3X were ordered according to their progression through cytokinesis. Asterisks mark GFP-LactC2 enrichment in the cell center before membrane invagination. Arrowheads label high GFP-LactC2 signals at the front of progressing membranes. (E) GFP-LactC2 enrichment at septum membranes compared with the plasma membrane. Measurements are based on clearly separated single septum membranes ($n = 49$). Scale bars: 2 μm. All quantifications are based on at least two independent experiments. Graphs display the mean; error bars represent SDs.

~10 μm (Supplemental Figure S2, C and D). Collectively, these observations suggest that PS is specifically polarized along the plasma membrane.

Our observation that PS was accumulating at sites of polarized growth prompted us to investigate whether this was the case in other states of cellular growth. GFP-LactC2 accumulated at the growing cell tip in two monopolar growing mutants *pom1Δ* (1.5-fold) and *tea1Δ* (1.7-fold) (Figure 3, A and E). In *tea1Δ* cells recovering from starvation, GFP-LactC2 rapidly localized to the new growing tip. Similar accumulation was also observed at the new tip of outgrowing spores (Figure 3, B, C, and E). We detected GFP-LactC2 accumulation at the tip of shmooing cells during mating, which was maintained during cell–cell contact (Figure 3D). Subsequently PS levels remained high at the site of fusion in zygotic stages even after fusion and became more evenly distributed after karyogamy (Figure 3, D and F). Thus the accumulation of PS at sites of polarization may be a general feature of the fission yeast life cycle.

PS polarization depends on actin-mediated endocytosis

We next asked which factors may contribute to polarize PS. Because the cytoskeleton is important for polarity positioning and maintenance, we first disassembled microtubules or F-actin using methyl-2-benzimidazol-2-yl-carbamate (MBC) or latrunculin A (LatA), respectively (Chang and Martin, 2009). Interestingly, we observed a near-complete loss of the GFP-LactC2 gradient after 30 min of LatA treatment (tip:side ratio ~1.1). By contrast, MBC had no effect on PS tip enrichment compared with controls (Figure 4A).

Because LatA treatment disassembles both actin patches and cables, which, respectively, contribute to endocytosis and transport, we used specific mutants affecting both processes individually. Strikingly, endocytic mutants such as *end4Δ* and *myo1Δ* exhibited a complete loss of PS polarity (tip:side ratio ~1.0; Figure 4B; Lee *et al.*, 2000; Iwaki *et al.*, 2004). A formin mutant, *for3Δ*, which lacks actin cables, displayed a reduced tip:side ratio but still maintained some level of PS polarization (Feierbach and Chang, 2001). Accordingly, a *myo51Δ myo52Δ* double mutant lacking type 5 myosins, which regulate vesicle trafficking along actin cables, had similar mild PS polarization defects as in *for3Δ* cells (Figure 4C; Win *et al.*, 2001). We also examined a temperature-sensitive allele of the exocyst subunit sec 8 (*sec 8-1*; Wang *et al.*, 2002), which blocks vesicle fusion, and detected a near-similar accumulation of GFP-LactC2 at cell tips as in the wild type (Figure 4D). Finally, we tested the role of the Rho GTPase Cdc42, which acts as a core regulator of polarity processes in fission yeast (Chang and Martin, 2009). Using both a temperature-sensitive mutant of orb6, *orb6-25*, an upstream regulator defective in Cdc42 polarization, or a hypomorphic allele of Cdc42 itself, *cdc42-1625*, we found a consistent mild reduction of the GFP-LactC2 gradient, similar to *for3Δ* mutants (Figure 4E; Martin *et al.*, 2007; Das *et al.*, 2009). Together these results suggest that PS

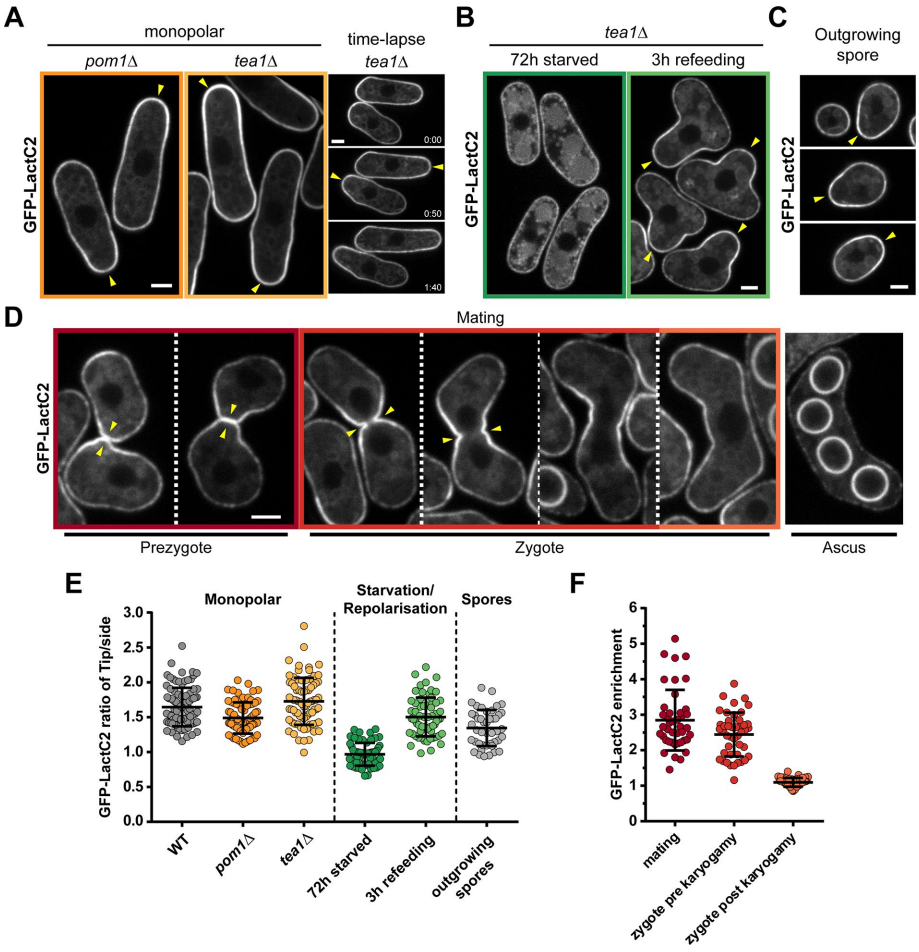

FIGURE 3: PS is polarized during cell growth, spore germination, and mating. (A) GFP-LactC2 expressed from pREP3X in monopolar mutants *pom1*Δ and *tea1*Δ. Left, representative images showing monopolar enrichment of GFP-LactC2. Arrowheads point at cell tips enriched in GFP-LactC2. Right, time-lapse images of *tea1*Δ cell growth. Arrowheads point to growing tips. (B) *tea1*Δ cells expressing shk1-GFP-LactC2 were grown and starved in YE5S for 72 h (left) and regrown in fresh YE5S for 3 h (right). Arrowheads point at GFP-LactC2 enrichment at the growing ends. (C) Spores from a wild-type h90 strain expressing shk1-GFP-LactC2 were germinated in YE5S at 25°C for 6 h and imaged. Arrowheads point at sites of GFP-LactC2 enrichment during outgrowth. (D) Mating of a wild-type h90 strain expressing shk1-GFP-LactC2 on ME agar for 16 h. Arrowheads point at regions of GFP-LactC2 enrichment. Scale bars: 2 µm. (E) Quantifications of GFP-LactC2 enrichment for experiments shown in A–C (wild type [WT] $n = 94$, *pom1*Δ $n = 80$, *tea1*Δ $n = 78$, starved $n = 62$, refed $n = 65$, spores $n = 44$). (F) Quantification of GFP-LactC2 enrichment during mating (mating $n = 42$, zygote pre $n = 44$, zygote post $n = 45$). For mating, enrichment of projection tip over the opposite cell side was measured. For zygotic stages, the intensity between cell center and end was quantified. All quantifications are based on at least two independent experiments. Graphs display the mean; error bars represent SDs.

accumulation at cell tips is predominantly generated by endocytosis, with some contribution from vesicle delivery.

PS and sterols may segregate into common membrane domains

The patterns of PS enrichment exhibited striking similarities with those reported for sterols, which are neutral lipids (Wachtler *et al.*, 2003). Both patterns are further disrupted in a *myo1*Δ mutant, which prompted us to investigate a potential connection between these two lipids (Figure 4B; Takeda and Chang, 2005). To test whether both lipids may be present in similar membrane regions, we stained sterol-rich regions with the dye filipin in cells expressing GFP-LactC2. This showed that these signals colocalized, suggesting that they might constitute a common membrane domain (Figure 5A). Next we investigated how disruption of either lipid would impact on the distribution of the other. We used ketoconazole to inhibit sterol synthesis, which is thought to abolish sterol polarization within 30 min (Martin and Konopka, 2004; Makushok *et al.*, 2016). Although we noted some high level of toxicity of this drug, with a significant fraction of cells dying upon treatment, this treatment led to a striking loss of GFP-LactC2 polarization both toward and within the plasma membrane in the fraction of surviving cells (Figure 5, B and C). In contrast, staining *pps1*Δ cells, which lack PS, with filipin did not reveal major defects in sterol-rich domain polarization (Figure 5D). These results suggest that sterols could direct the tip enrichment of PS.

PS may contribute to establish a gradient of negative charges along the plasma membrane

PS is the most abundant negatively charged lipid in the plasma membrane. Given our findings that PS is polarized, we asked whether this polarization may generate a gradient of net negative charges along the membrane. To this end, we cloned a set of membrane-charge probes consisting of a GFP fused to the human K-Ras C-terminus bearing different net charges of 2+, 4+, 6+, and 8+ into an inducible plasmid (Roy *et al.*, 2000). As expected, when expressed in the wild type, these probes were targeted to the plasma membrane as well as internal membranes (Figure 6A). Interestingly, we found that sensors with increasing positive charges were increasingly accumulated to the plasma membrane with respect to endomembranes. GFP-8+ was the most enriched charge probe at the plasma membrane, with a level similar to the PIP_2 probe but to a lesser extent than the PS probe (Figure 6, A and B). These observations, which are consistent with findings in mammalian cells, suggest that these probes may be functional in *S. pombe* (Yeung *et al.*, 2008).

Next we investigated the polarization of those probes along the plasma membrane, by computing a tip:side intensity ratio. We found that this ratio progressively increased from the 2+ probe (ratio ~1.0) to the 8+ probe (ratio ~ 1.3) (Figure 6, A and C). The 8+ probe was more enriched at cell tips than the PIP_2 probe but to a lesser extent than the PS probe. To directly test whether PS gradients contribute to this charge gradient, we first treated cells with LatA to abolish PS enrichment. We found that the gradient of GFP-8+ was completely abolished upon 30 min of LatA treatment, in a similar manner to GFP-LactC2 (Figures 6D and 4A). We also monitored the localization of GFP-8+ in the *pps1*Δ mutant. This revealed a marked reduction of both tip accumulation and plasma membrane

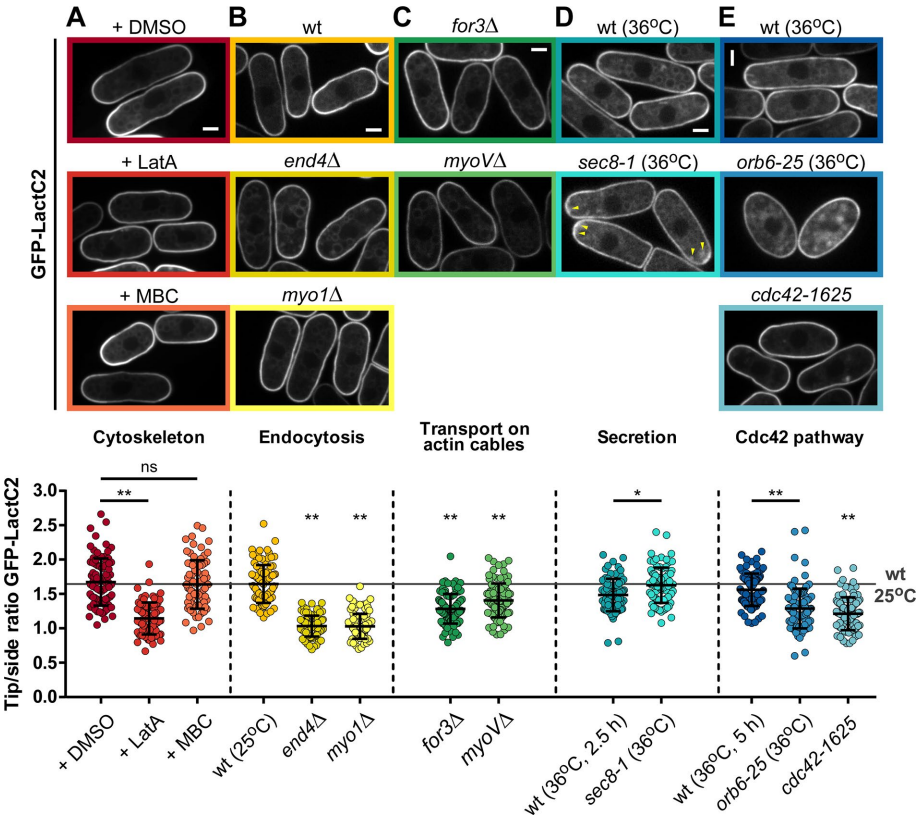

FIGURE 4: Contribution of endocytosis, transport, and cdc42 to PS polarization. Top, representative images of GFP-LactC2 distribution in the indicated conditions. Bottom, quantification of tip:side ratio of GFP-LactC2. (A) Wild-type (wt) cells expressing GFP-LactC2 were treated with either 1% DMSO ($n = 85$), 100 µM LatA ($n = 84$), or 130.8 µM MBC ($n = 78$). There was a statistically significant difference between those groups as determined by one-way ANOVA ($F(2, 244) = 89.03$, $p < 0.0001$). (B) GFP-LactC2 distribution in wild type ($n = 94$) and endocytotic mutants *end4Δ* ($n = 94$) and *myo1Δ* ($n = 91$). (C) GFP-LactC2 distribution in actin-cable transport mutants *for3Δ* ($n = 100$) and *myoVΔ* ($n = 96$). (D) GFP-LactC2 distribution in wild type ($n = 82$) and temperature-sensitive exocyst mutant *sec 8-1* ($n = 90$) after 2.5 h at 36°C. Arrowheads point at GFP-LactC2 dot accumulations under the plasma membrane at cell tips. (E) GFP-LactC2 distribution in wild type ($n = 101$) and temperature-sensitive mutant *orb6-25* ($n = 100$) after 5 h at 36°C and *cdc42-1625* ($n = 90$) at 25°C. For wild type, *end4Δ*, *myo1Δ*, *for3Δ*, *myoVΔ*, and *cdc42-1625*, there was a statistically significant difference between groups as determined by one-way ANOVA ($F(5, 559) = 105.0$, $p < 0.0001$). All strains express GFP-LactC2 from the inducible pREP3X plasmid. Scale bars: 2 µm. All quantifications are based on at least two independent experiments. Graphs display the mean; error bars represent SDs. Two-tailed, unpaired *t* test: *, $p = 0.0002$; **, $p < 0.0001$.

recruitment of the probe, suggesting PS may dominantly contribute to localize this charged probe along the plasma membrane (Figure 6E). Together these findings support the existence of a gradient of negative charges along the plasma membrane that may be primarily set by PS distribution.

Influence of PS on Rho GTPase recruitment and polarization

It has been suggested that the localization of proteins with polybasic clusters/positive charges, like Rho GTPases, is influenced by charged lipids and consequent membrane electrostatics (Heo *et al.*, 2006; Yeung *et al.*, 2008; Li *et al.*, 2014). Given the polarization of PS and negative charges and that many Rho GTPases localize to sites of polarized growth, we asked how PS and charges may affect Rho GTPase recruitment. To this end, we investigated the localization of two Rho GTPases, Cdc42 and Rho1, which respectively regulate actin assembly and cell wall synthesis (Arellano *et al.*, 1996; Nakano *et al.*, 1997; Estravis *et al.*, 2011). Fission yeast Cdc42 has a polybasic stretch with a net charge of 3+ close to its C-terminus, and this charge has been suggested to affect its plasma membrane enrichment in budding yeast (Das *et al.*, 2012).

When we compared the localization of PS and Cdc42-mCherry^{SW}, we found that both signals labeled the same set of membranes, with the exception of the nuclear envelope, which was only marked by Cdc42-mCherry^{SW} (Figure 7A). However, Cdc42-mCherry^{SW} was less enriched at the plasma membrane than GFP-LactC2. We found a clear correlation between the levels of the two signals along the plasma membrane, which suggests that the abundance of Cdc42 at the plasma membrane may be linked to PS levels in a dose-dependent manner (Figure 7B).

We then asked how PS may influence the subcellular localization of Cdc42-mCherry^{SW} and GFP-Rho1. These two proteins carry C-terminal net charges of 3+ and 7+, respectively, allowing us to distinguish potential stereospecific from electrostatic effects of PS. We first analyzed the tip gradient of both proteins and compared them with that of GFP-LactC2. The profile of Cdc42-mCherry^{SW} dropped sharply from the tip, as reported previously, with a tip enrichment of 1.9-fold (Figure 7, C–E; Bendezu *et al.*, 2015). In contrast, the GFP-Rho1 tip maximum was wider and plateaued for ~1.5 µm and exhibited a tip enrichment of 1.8-fold. Interestingly, this pattern is closer to the profile of GFP-LactC2, which has a tip signal plateau of ~2.5 µm (Figure 7, C–E). Because both GTPases had similar tip enrichments, we asked whether they might be differentially influenced by the lack of PS. Remarkably, although the tip:side ratio of Cdc42-mCherry^{SW} was only mildly affected in *pps1Δ* cells (1.8-fold), GFP-Rho1 enrichment was more strongly reduced to 1.4-fold (Figure 7, C and E). This suggests that PS contributes to the localization of charged proteins along the plasma membrane. Next we asked whether PS loss would similarly impact the global enrichment in the plasma membrane (1.3-fold for both proteins). We found again a stronger effect on GFP-Rho1 than on Cdc42-mCherry^{SW} in *pps1Δ* cells (Figure 7F), implying that PS also contributes to the plasma membrane retention of these proteins.

Taken together, these results suggest that PS influences the polarization of Rho1 and Cdc42 and possibly other charged membrane factors in fission yeast in a protein charge–dependent manner.

Influence of PS on cell polarity and morphogenesis

We then investigated the contribution of PS to general polarized behavior and morphogenesis. We first grew *pps1Δ* cells at different temperatures and assayed defects in cell shape. At lower temperatures, *pps1Δ* exhibited longer length than the wild type (14.3 ± 1.2 µm in wild type vs. 16.3 ± 1.5 µm in *pps1Δ*) but similar diameter (Figure 8, A–C). At higher temperatures, however, *pps1Δ* cells

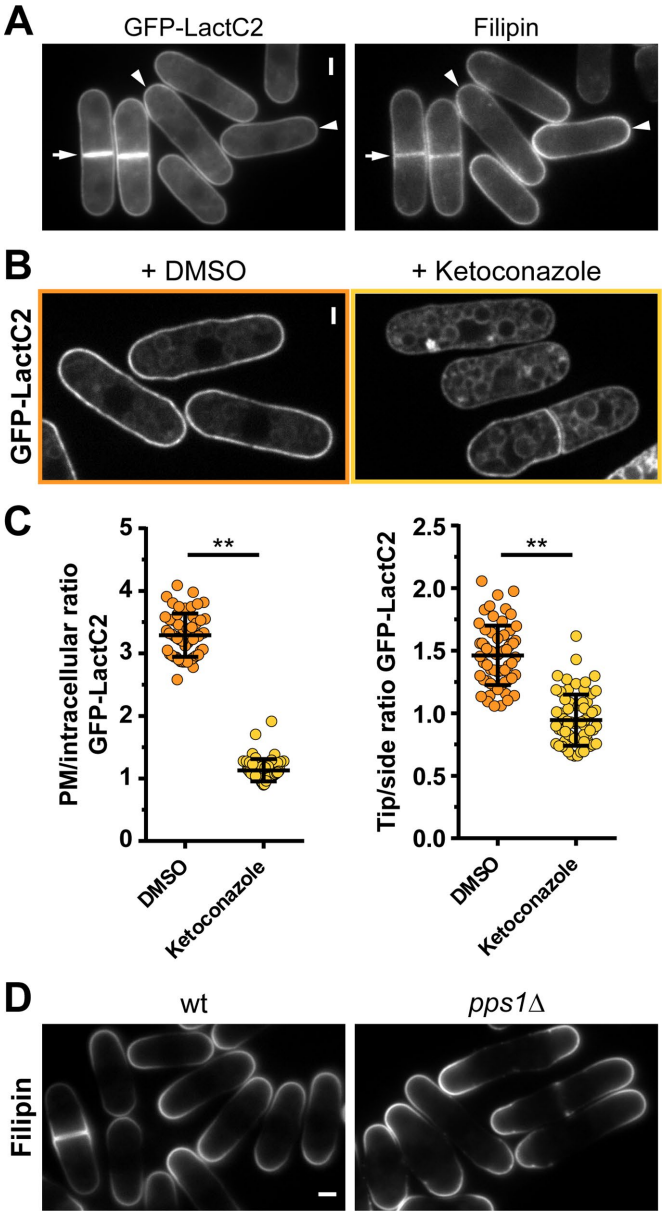

FIGURE 5: PS and sterols may constitute a common membrane domain. (A) Epifluorescence images of cells expressing GFP-LactC2 from a pREP3X plasmid and stained with filipin. Colocalization of signals at cell tips (arrowheads) and sites of cytokinesis (arrows). (B) Cells expressing shk1-GFP-LactC2 were treated with DMSO or 400 µM ketoconazole for 30 min. (C) Quantification of GFP-LactC2 enrichment after ketoconazole treatment for 30 min. Left, plasma membrane enrichment (DMSO $n = 55$, ketoconazole $n = 57$). Right, tip:side ratio (DMSO $n = 63$, ketoconazole $n = 67$). (D) Sterol-rich domains stained with filipin in wild-type (wt) and *pps1*Δ cells. Two-tailed, unpaired *t* test: **, $p < 0.0001$. Scale bars: 2 µm. All quantifications are based on at least two independent experiments. Graphs display the mean; error bars represent SDs.

became stubbier compared with the wild type (Figure 8, A and B). We also imaged the actin cytoskeleton with phalloidin staining. At 25°C, *pps1*Δ cells exhibited more dispersed endocytic patches than wild-type cells but similar actin cables (Figure 8D). At 35°C, however, *pps1*Δ cells had an overall reduced number of actin patches (Figure 8D and Supplemental Figure S3). Thus PS may influence cell dimensions and actin organization.

To test the implication of PS in polarization processes, we next performed growth time lapses to investigate NETO patterns. Interestingly, we found that, in a *pps1*Δ mutant, NETO occurred prematurely in 44% of cells (wild type: 14%) in a similar manner as other known mutants connected to cell polarization (Figure 8E; Feierbach and Chang, 2001; Das *et al.*, 2007). To further assay the role of PS in bipolar growth, we crossed *pps1*Δ with the monopolar, T-shaped mutant *tea4*Δ, starved these cells, and let them repolarize in fresh media. In *tea4*Δ, we observed that most cells grew only from a single site, frequently branching from the cell sides. In contrast, *pps1*Δ cells showed no evidence of branching, and almost all cells immediately grew in a bipolar manner upon recovery. Interestingly, in ~50% of the cells of the double mutant *pps1*Δ *tea4*Δ, we observed two tips growing at the same time (Figure 8, F and G). We conclude that PS may contribute to regulate cell polarity by restricting or delaying bipolar growth.

DISCUSSION

PS forms a polarized membrane domain at sites of cell growth and division

We used a GFP-LactC2 probe to determine the pattern of localization of PS during the fission yeast cell cycle. We found a striking enrichment of PS at sites of polarized cell growth during interphase, spore outgrowth, and at mating tip projections. This pattern is reminiscent of sterol-rich domains, suggesting that the fission yeast membrane can organize into lateral domains containing multiple types of lipids (Wachtler *et al.*, 2003). Indeed, we found that both lipids colocalize, and analysis of their interdependence suggests that the presence of sterols may be required for tip enrichment of PS, but not vice versa. Likewise, in mammalian cells, high content of cholesterol has been associated with a reduced PS diffusion rate, and cells with low PS levels exhibit normal cholesterol levels and localization but altered bilayer distribution. In addition, PS and cholesterol have also been shown to coalesce in model membranes and lipid rafts (Pike *et al.*, 2005; Kay *et al.*, 2012; Maekawa and Fairn, 2015). Thus the connection between sterol and PS may be a general feature of eukaryotic membranes.

As for sterol-rich domains, we found that PS polarization along the plasma membrane depends on endocytosis. As previously reported in budding yeast, this enrichment could be caused by the exclusion of PS from endocytic vesicles that form mainly at cell tips (Fairn *et al.*, 2011a). In contrast, while the exocyst complex appears to be required for PS polarization in budding yeast, it is mostly dispensable in fission yeast (Fairn *et al.*, 2011a). In *sec 8-1* mutants, we observed dots of GFP-LactC2 that accumulated underneath the plasma membrane in delayed fusion (Figure 4D). A possibility is that, unlike in budding yeast, other membrane fusion mechanisms independent of the exocyst may be active in fission yeast, as several exocyst mutants are still able to grow in a polarized manner (Bendezu and Martin, 2011). These findings highlight how different architectures of polarized trafficking may affect lateral membrane organization.

PS sustains transcellular charge gradients and Rho GTPase localization

Using a suite of membrane charge probes, we also examined the spatial organization of membrane charges in fission yeast. Similar to previous findings in human cells, endomembranes in our study were usually less negatively charged than the plasma membrane (Yeung *et al.*, 2008). This suggests that generic principles of membrane electrostatics may be conserved from yeast to humans. In addition, we also discovered that charges at the plasma membrane may form

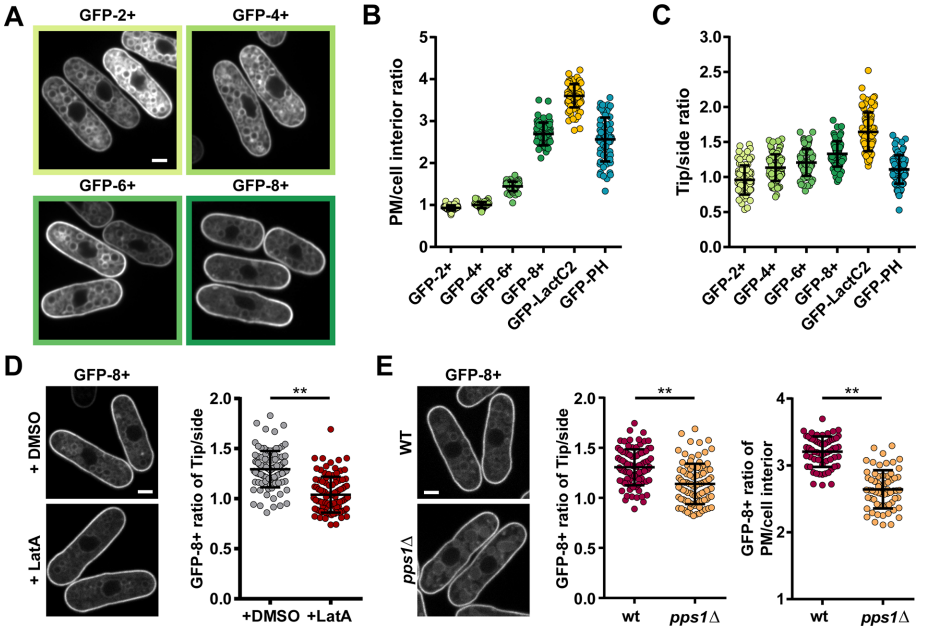

FIGURE 6: PS gradients may set a transcellular membrane charge gradient. (A) Distribution of membrane charge probes GFP-2+, 4+, 6+, and 8+ expressed from an inducible pREP3X plasmid in wild-type cells. (B) Quantification of plasma membrane enrichment over cell interior for membrane charge probes and charged lipid probes (GFP-2+, 4+, and 6+ $n = 60$, GFP-8+ $n = 59$, GFP-LactC2 $n = 94$, GFP-PH $n = 61$). (C) Quantification of cell tip over cell side enrichment at the plasma membrane for membrane charge probes and charged lipid probes (GFP-2+ $n = 83$, GFP-4+ $n = 84$, GFP-6+ $n = 86$, GFP-8+ $n = 72$, GFP-LactC2 $n = 94$, GFP-PH $n = 87$). (D) Impact of LatA treatment on the distribution of the GFP-8+ probe expressed from the pREP3X plasmid. Representative images (left) and quantification of the tip:side ratio on the plasma membrane (right; DMSO $n = 100$, LatA $n = 98$). (E) Comparison of GFP-8+ probe distribution expressed under the shk1 promotor in wild-type and *pps1*Δ cells. Left, representative images. Center, quantification of the tip:side ratio on the plasma membrane (wt $n = 89$, *pps1*Δ $n = 92$). Right, quantification of the plasma membrane/cell interior ratio (wt $n = 61$, *pps1*Δ $n = 63$). Two-tailed, unpaired *t* test: **, $p < 0.0001$. Scale bars: 2 μm. All quantifications are based on at least two independent experiments. Graphs display the mean; error bars represent SDs.

a gradient, with the tip being more negatively charged than the cell sides. This pattern also depends on actin and relies on the presence of PS, suggesting that PS spatial distribution may promote an electrostatic gradient along the cell long axis (Yeung *et al.*, 2008). This gradient may fill multiple functions. Membrane charges are important for the targeting of proteins, especially to regions of high charge like the plasma membrane (Heo *et al.*, 2006; Yeung *et al.*, 2008). We propose that PS contributes to the stabilization of positively charged Rho GTPases at cell tips. As Rho1, which bears more positive charge at its C-terminus (net charge 7+), was more delocalized than the less charged Cdc42 (net charge 3+) in cells lacking PS, we suggest that this effect may reflect nonspecific electrostatic interactions with PS. The observed changes in patterning of Rho1, the catalytic subunit of the cell wall synthases, are likely functionally relevant, as *pps1*Δ cells have been previously suggested to have cell wall integrity defects (Matsuo *et al.*, 2007).

Taken together, this work adds to an understanding of the role of nonspecific contribution of charges to the spatial organization of many functional layers inside cells (Simons *et al.*, 2009; Das *et al.*, 2012; Chang and Minc, 2014; Haupt *et al.*, 2014).

PS regulates growth from new polarization sites

An interesting observation was to find that a *pps1*Δ mutant, which lacks PS, undergoes premature NETO, switching to bipolar growth immediately after cytokinesis. This phenotype is further supported by the presence of bipolar tip growth in *pps1*Δ *tea4*Δ cells that partially suppress the monopolar phenotype of *tea4*Δ cells. This suggests that PS possibly functions to negatively regulate bipolar growth independent of the Tea1/Tea4 pathway. Premature NETO phenotypes have also been reported for other mutants connected to Cdc42 and Rho1, such as the formin *for3*Δ and *rga4*Δ, a Rho GAP for Cdc42, and other Rho GTPases like Rho2, which is connected to Rho1 (Feierbach and Chang, 2001; Das *et al.*, 2007; Tatebe *et al.*, 2008; Soto *et al.*, 2010). Thus these reports suggest that the role of PS in bipolar growth could potentially be enacted through the proper regulation of GTPase localization and dynamics at the membrane. Further work connecting lipid domains and membrane electrostatics to cell polarity will provide important information on the contribution of nonspecific versus specific layers of regulation of cellular spatial organization.

MATERIALS AND METHODS

Yeast strains, genetic methods, and media

Standard methods for *S. pombe* media and genetic manipulations were used (www-bcf.usc.edu/~forsburg; www.biotwiki.org/foswiki/bin/view/Pombe/NurseLabManual). Strains used in this study are listed in Table 1.

Plasmid and strain generation

GFP-LactC2 and GFP-LactC2-AAA cloning into pREP3X. For cloning into the pREP3X vector, the GFP-LactC2 or GFP-LactC2-AAA open reading frame (ORF) from pEGFP-C1 vector (Yeung *et al.*, 2008) was amplified by PCR, adding *Sal*I restriction sites to the 5′ and 3′ end. The PCR product and pREP3X were subsequently digested with *Sal*I, ligated, and transformed into *Escherichia coli*. Positive clones were sequence verified.

Membrane charge–sensor cloning into pREP3X. ORFs of membrane-charge sensors were amplified by PCR from pcDNA3 (Roy *et al.*, 2000), with simultaneous addition of restriction sites that were then used for subcloning into pREP3X. Sites were the same for GFP-8+ and 2+ (5′ *Xho*I, 3′ *Bam*HI) and GFP-6+ and 4+ (5′ *Sal*I, 3′ *Sma*I). Positive clones were sequence verified.

Cloning of GFP-LactC2, GFP-8+ and GFP-rho1 for stable integration. The goal was to generate constitutive expression constructs of GFP-LactC2, GFP-8+, and GFP-rho1 with shk1 promotor and nmt1 terminator. For GFP-LactC2 and GFP-8+, first, the ORF and nmt1 terminator were PCR amplified (introducing a 5′ *Nde*I site) from pREP3X vectors containing the respective ORF (forward: 5′-ACAAGATAACATATGGTGAGCAAGGGCGAG-3′; reverse: 5′-AAAAAACAATTGCCGAGTGGTTAAGGAGTTAGACT-3′). A *Sac*I site was already present at the end of the nmt1 terminator of pREP3X. PCR product and target vector (pBSSK+ura4+-shk1promotor:ScGic2CRIB:GFP3:nmt1term; Tatebe *et al.*, 2008), were digested with *Nde*I and *Sac*I. The vector backbone was retained, now lacking the CRIB-3GFP and nmt1 terminator part. Insert and backbone were ligated, yielding

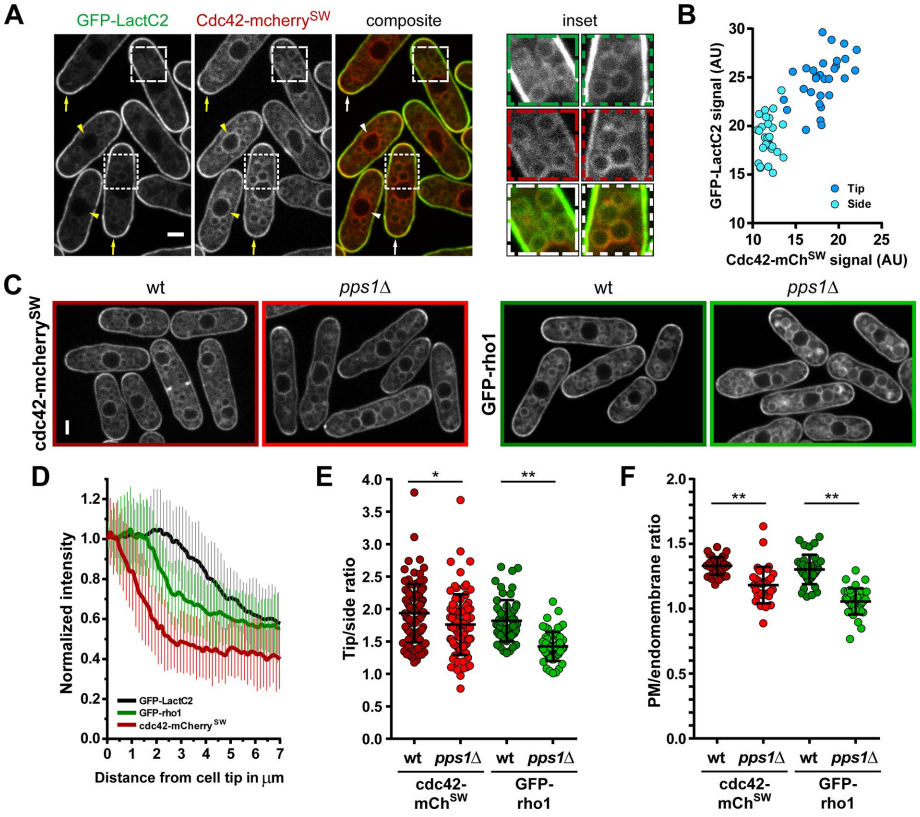

FIGURE 7: A PS-deficient mutant affects rho1 and cdc42 localization. (A) Comparison of signals of GFP-LactC2 and cdc42-mcherry^{SW}. Left, overview highlighting cell tip coenrichment (arrows) and nuclear envelope signal (arrowheads). Right, enlargements of subcellular regions show overlap of endomembrane signals. (B) Correlation of GFP-LactC2 and cdc42-mcherry^{SW} signals measured at cell tips and sides. (C) Distribution of cdc42-mcherry^{SW} (left, red frames) and GFP-rho1 (right, green frames) in wild-type and *pps1*Δ cells. (D) Average signal gradient emanating from cell tips for GFP-LactC2 ($n = 39$), GFP-rho1 ($n = 42$), and cdc42-mcherry^{SW} ($n = 41$). (E) Tip:side ratio of cdc42-mcherry^{SW} and GFP-rho1 in wild-type (cdc42 $n = 98$, rho1 $n = 58$) and *pps1*Δ (cdc42 $n = 86$, rho1 $n = 60$) cells. (F) Plasma membrane:endomembrane ratio of cdc42-mcherry^{SW} and GFP-rho1 in wild-type (cdc42 $n = 36$, rho1 $n = 38$) and *pps1*Δ (cdc42 $n = 33$, rho1 $n = 39$) cells. Two-tailed, unpaired *t* test: **, $p < 0.0001$; *, $p = 0.0098$. Scale bars: 2 μm. All quantifications are based on at least two independent experiments. Graphs display the mean; error bars represent SDs.

a construct containing the shk1 promotor, the ORF, and the nmt1 terminator. Because the LactC2 ORF contained a *Stu*I site, this vector could not be linearized in the *ura4+* cassette. Consequently both constructs were subcloned into pJK148 via *Apa*I and *Sac*I sites. All cloning steps were monitored by sequencing. *GFP-rho1* was cloned by stitching of PCR fragments. The *rho1* ORF was derived from pARTGFPrho1 plasmid (Nakano *et al.*, 1997). The shk1 promoter was amplified from pBSSK+ura4+-shk1promoter:ScGic2CRIB:GFP3:nmt 1term to carry a *Pst*I restriction site at the 5′ end and the first 12 base pairs of the GFP-rho1 ORF at the 3′ (forward: 5′-AAAAAACTGCAG-TCTAACAAAGAAACCTGAC-3′; reverse: 5′-CTTGCTCACCATAG-TAAATAAATTTATTAACG-3′). The GFP-rho1 ORF was amplified from a pREP41X GFP-rho1 vector to carry the last 12 base pairs of the shk1 promoter at the 5′ end and a *Sac*I site intrinsic to the nmt1 terminator at the 3′ end (forward:5′-AATTTATTTACTATGGTGAGCAAGGG-CGAG-3′; reverse:5′-AAAAAACAATTGCCGAGTGGTTAAGGAGTT-AGACT-3′). These two fragments were mixed in equal amounts and PCR amplified with forward primer of the previous shk1 reaction and reverse primer of the previous GFP-rho1 reaction, yielding the expression cassette that was cloned into pJK148 via *Pst*I and *Sac*I restriction sites.

Transformation of cells. Plasmid transformations were carried out using the Frozen-EZ Yeast Transformation II Kit (Zymo Research, Irvine, CA). pJK148-based constructs were linearized with *Nru*I before transformation by the lithium acetate procedure (Gietz *et al.*, 1995).

Generation of a pps1::NatMX deletion strain. Deletion of the entire *pps1*$^{+}$ ORF and its replacement by the NatMX cassette was achieved by a PCR-based approach (Bahler *et al.*, 1998; Sato *et al.*, 2005). The deletion cassette was generated with forward primer (5′-GGTGCCTTATTTTTGTTAG-TTATTCGACTTCCGGTAAATAAACAGG-TACAATTAGAACCAGAAACTGC-CAATTTTGGAAGCGGATCCCCGGGTTA-ATTAA-3′), reverse primer (5′-TGTGTATA-CCCAGATCGCTGTACTGTAAAGTTTCATT TGGATTCTATTGAATAAAAGCATCAGTT-GATCAAACTAAAAAAGAATTCGAGCTC-GTTTAAAC-3′), and pFA6-NatMX plasmid. Wild-type *S. pombe* cells were transformed using the lithium acetate procedure. Deletion was verified by PCR.

Growth of cells and induction

Cells were generally grown at 25°C in yeast extract + 5 supplements (YE5S) in overnight cultures unless stated otherwise. For strains with a *pps1*Δ genotype, YE5S was supplemented with 1 mM ethanolamine (Sigma-Aldrich, St. Louis, MO) to allow synthesis of PS metabolites, as previously reported (Matsuo *et al.*, 2007). For starvation experiments, cells were grown at 25°C in YE5S for 72 h, washed once in 1 ml fresh medium, diluted 1:25 into fresh medium, and regrown for at least 3 h. For analysis of mating, an h90 strain was placed on malt extract (ME) agar for 16 h. Cells were then transferred to an ME agar pad, and stages of mating imaged. For inducing expression from the pREP3X plasmid, cells were grown at 25°C in Edinburgh minimal medium (EMM) with appropriate supplements but without thiamine for 40–48 h and kept in exponential growth phase by appropriate dilution, unless stated otherwise.

Pharmacological inhibition and staining

MBC (Sigma-Aldrich) was used at a final concentration of 130.8 μM (25 μg/ml) from a 100× stock solution made fresh in dimethyl sulfoxide (DMSO; Sigma-Aldrich). LatA (Sigma-Aldrich) was used at a final concentration of 100 μM from a 100× stock in DMSO. For staining of growing cell ends, calcofluor was added to a cell suspension at a final concentration of 54.4 μM (50 μg/ml) from a 100× stock solution and incubated for 1 min, and cells were concentrated and imaged immediately. For sterol-rich membrane domain staining, a fresh aliquot of 7.6 mM filipin (5 mg/ml; Sigma-Aldrich) in DMSO was diluted 1:5 in DMSO and added to the cell suspension at 1/100. Cells were concentrated and imaged within 5 min. Ketoconazole (Sigma-Aldrich) was used at a final concentration of 400 μM from a freshly prepared 30 mM stock solution in DMSO and added to cells for 30 min before

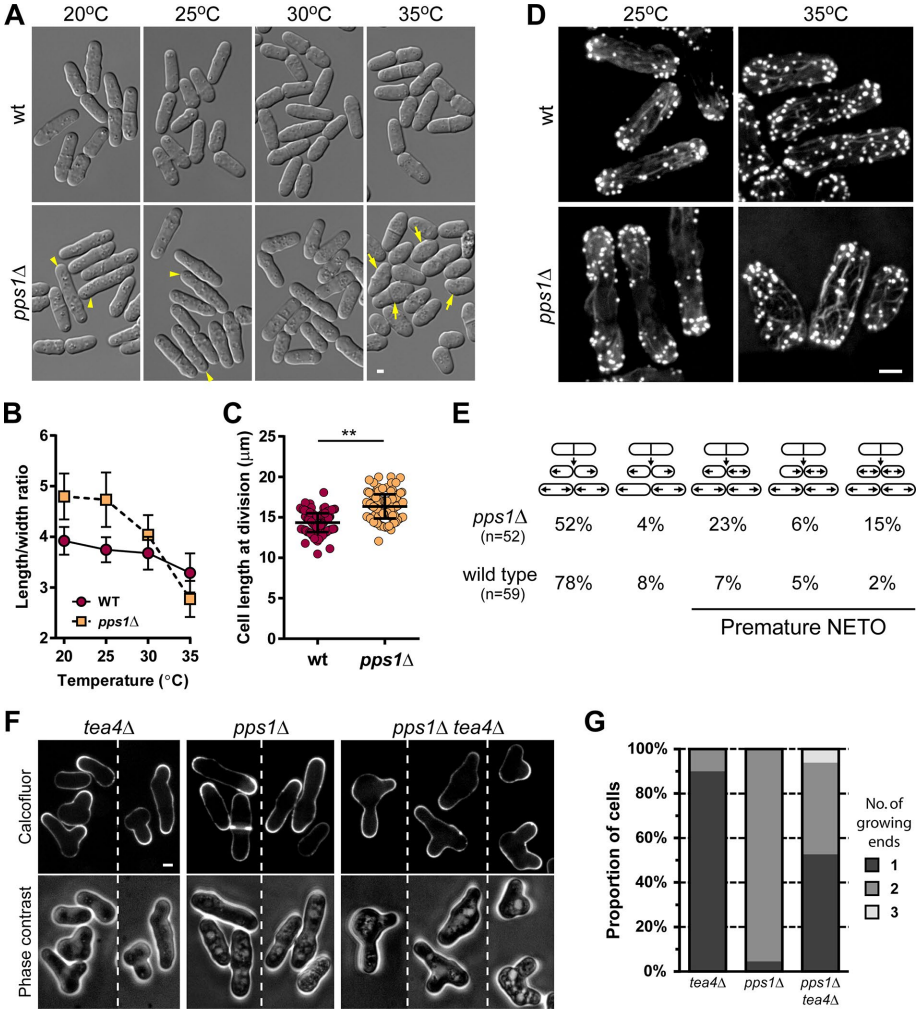

FIGURE 8: Cells without PS have defects in cell shape and patterns of polar growth. (A) Wild-type and *pps1*Δ cells grown at 20, 25, 30, and 35°C. Arrowheads point to elongated cells with high aspect ratio and arrows to stubby cells with low aspect ratio. (B) Quantification of aspect ratios of wild-type and *pps1*Δ cells grown at different temperatures. For each time point, 44–47 cells were analyzed. (C) Quantification of cell length at cell division at 25°C of wild-type ($n = 141$) and *pps1*Δ ($n = 126$) cells. Two-tailed, unpaired *t* test: **, $p < 0.0001$. (D) Alexa Fluor 488–phalloidin staining of wild-type and *pps1*Δ cells grown at 25 and 35°C. Images are maximum-intensity projections of whole cell z-stacks with 0.1 μm step size. (E) Growth pattern analysis of wild-type and *pps1*Δ cells determined by differential interference contrast live-cell imaging. (F) Polarity reestablishment after starvation. Growth zones were visualized by calcofluor staining after 6 h (*tea4*Δ) or 4 h (*pps1*Δ and *tea4*Δ *pps1*Δ) of growth in fresh medium. (G) Quantification of the number of growth zones after recovery from starvation of *tea4*Δ, *pps1*Δ,and *tea4*Δ *pps1*Δ cells ($n = 180$, 156, and 131, respectively). Scale bars: 2 μm. All quantifications, except in G, are based on at least two independent experiments. Graphs display the mean; error bars represent SDs.

observation, following a protocol previously established for *Candida albicans* cells (Martin and Konopka, 2004). Note that this treatment caused cell death in ~50–60% of the cells. Lower concentrations had no significant effect on PS polarization. Actin staining with Alexa Fluor 488–phalloidin (Life Technologies, Carlsbad, CA) was performed as previously described, but PEM buffer (0.1 M PIPES, pH 6.8, 1 mM ethylene glycol-bis(β-aminoethyl ether)-*N*,*N*,*N*′,*N*′-tetraacetic acid [EGTA], 1 mM $MgCl_2$) was used (Martin *et al.*, 2007).

Microscopy

For instantaneous imaging, 1.8 μl of fresh, concentrated cells were placed between a glass slide and coverslip and imaged within 20 min. For long-term imaging, cells were placed on 2% agar YE5S pads and covered with a coverslip. Cells were imaged at room temperature (23–25°C), with controlled humidity, with an inverted spinning-disk confocal microscope equipped with a motorized stage and automatic focus (Nikon Ti-Eclipse), a Yokogawa CSUX1FW spinning unit, and an EM-CCD camera (Hamamatsu). Images were acquired with a 100× oil-immersion objective (Nikon CFI Plan Apo DM 100×/1.4 NA) with a 2.5× magnifying lens or a 100× objective alone.

Image analysis

Quantitative image analysis was done using ImageJ (National Institutes of Health, Bethesda, MD). We analyzed growing interphase cells that were selected based on visual inspection. Mitotic cells were excluded based on nuclear morphologies (elongated; two nuclei) that were negatively stained by all probes and membrane invaginations during septation. For plasmid-expressing cells, we excluded cells with much stronger signal than their neighboring cells. For each experiment, cells from >10 fields were measured. For tip:side ratios at the plasma membrane, the entire cell pole of the old end and a similar-sized region on the cell side on the right of the tip were measured. In cells expressing Cdc42-mcherry^{SW}, tip:side quantifications were done measuring the very narrow region of maximal Cdc42-mcherry^{SW} signal at the old end and a broader region on the side. For plasma membrane:cell interior ratios, the entire plasma membrane and the remaining intracellular signal were measured. The latter was routinely measured without the nuclear volume, which was usually devoid of signal, except in *pps1*Δ and GFP-LactC2-AAA–expressing cells. For measurements of plasma membrane:endomembrane ratios of GFP-Rho1 and Cdc42-mcherry^{SW}, the average intensity of the plasma membrane was compared with the average intensity of 5–10 well-distinguished intracellular membranes. Images used in the figures were intensity-level optimized in the whole field of view and comparably within panels.

Statistical analysis

Statistical analyses were carried out using Prism 6 software (GraphPad Software, La Jolla, CA). We used a two-tailed, unpaired *t* test to compare pairs of experimental conditions. For three or more experiments, we used one-way analysis of variance (ANOVA) followed by Dunnett multiple comparisons test. Statistically significant difference between groups are *$p < 0.001$ or **$p < 0.0001$, unless stated otherwise.

Strain	Genotype
NM291	*h- ade6-210 leu1-32 ura4-D18*
AH10	*h+ ade6-210 leu1-32 ura4-D18 [pREP3X-GFP-LactC2:leu1+]*
AH92	*h- pps1::NatMX ade6-210 leu1-32 ura4-D18*
AH159	*h+ leu1-32::pJK148-shk1-GFP-LactC2-nmt1-leu1+ ade6-210 leu1-32 ura4-D18*
AH180	*h90 leu1-32::pJK148-shk1-GFP-LactC2-nmt1-leu1+ leu1-32 ura4-D18*
AH170	*h+ pps1::NatMX leu1-32::pJK148-shk1-GFP-LactC2-nmt1-leu1+ ade6-210 leu1-32 ura4-D18*
AH208	*h+ leu1-32::pJK148-shk1-GFP-8+-nmt1-leu1+ ade6-210 leu1-32 ura4-D18*
AH215	*pps1::NatMX leu1-32::pJK148-shk1-GFP-8+-nmt1-leu1+ ade6-210 leu1-32 ura4-D18*
AH119	*h+ tea1::ura ade6-210 leu1-32 ura4-D18 [pREP3X-GFP-LactC2:leu1+]*
AH181	*tea1::NatMX leu1-32::pJK148-shk1-GFP-LactC2-nmt1-leu1+*
AH183	*pom1::NatMX [pREP3X-GFP-LactC2:leu1+]*
AH39	*h+ end4::KanMX [pREP3X-GFP-LactC2:leu1+]*
AH38	*h+ myo1::KanMX [pREP3X-GFP-LactC2:leu1+]*
AH193	*h- for3::KanMX [pREP3X-GFP-LactC2:leu1+]*
AH216	*h90 myo51::ura myo52::ura [pREP3X-GFP-LactC2:leu1+]*
AH86	*sec 8-1 leu1-32::pJK148-nmt1-GFP-LactC2-nmt1-leu1+*
AH194	*orb6-25 [pREP3X-GFP-LactC2:leu1+]*
AH51	*cdc42-1625:KanMX [pREP3X-GFP-LactC2:leu1+]*
AH187	*cdc42-mCherry^{SW}-KanMX leu1-32::pJK148-shk1-GFP-LactC2-nmt1-leu1+*
AH188	*pps1::NatMX cdc42-mCherry^{SW}-KanMX leu1-32::pJK148-shk1-GFP-LactC2-nmt1-leu1+*
AH262	*h+ leu1-32::pJK148-shk1-GFP-rho1-nmt1-leu1+ ade6-210 leu1-32 ura4-D18*
AH263	*pps1::NatMX leu1-32::pJK148-shk1-GFP-rho1-nmt1-leu1+*
DB162	*h+ tea4::KanMX*
AH214	*pps1::NatMX tea4::KanMX*
AH192	*h+ ade6-210 leu1-32 ura4-D18 [pREP3X-GFP-LactC2-AAA]*
AH73	*h+ ade6-210 leu1-32 ura4-D18 [pREP1-GFP-PH]*
AH47	*h+ ade6-210 leu1-32 ura4-D18 [pREP3X-GFP-2+]*
AH48	*h+ ade6-210 leu1-32 ura4-D18 [pREP3X-GFP-4+]*
AH49	*h+ ade6-210 leu1-32 ura4-D18 [pREP3X-GFP-6+]*
AH50	*h+ ade6-210 leu1-32 ura4-D18 [pREP3X-GFP-8+]*

TABLE 1: Strains used in this study.

ACKNOWLEDGMENTS

We thank members of the Minc laboratory for technical help and discussion and the ImagoSeine core facility of the Institut Jacques Monod, also associated with Infrastructures en Biologie Santé et Agronomie (IBiSA) and France BioImaging infrastructures. We thank S. Grinstein, T. Kuno, J. Silvius, S. Martin, and K. Nakano for providing us with plasmids and strains. This work is supported by the Centre National de la Recherche Scientifique (CNRS) and grants from the Mairie de Paris emergence program and the Career Integration Grant (CIG) program of the European Community (EC) and the Initial Training Network (ITN) consortium FungiBrain.

REFERENCES

Arellano M, Duran A, Perez P (1996). Rho 1 GTPase activates the (1-3) beta-D-glucan synthase and is involved in *Schizosaccharomyces pombe* morphogenesis. EMBO J 15, 4584–4591.

Bahler J, Wu JQ, Longtine MS, Shah NG, McKenzie A 3rd, Steever AB, Wach A, Philippsen P, Pringle JR (1998). Heterologous modules for efficient and versatile PCR-based gene targeting in *Schizosaccharomyces pombe*. Yeast 14, 943–951.

Bendezu FO, Martin SG (2011). Actin cables and the exocyst form two independent morphogenesis pathways in the fission yeast. Mol Biol Cell 22, 44–53.

Bendezu FO, Vincenzetti V, Vavylonis D, Wyss R, Vogel H, Martin SG (2015). Spontaneous Cdc42 polarization independent of GDI-mediated extraction and actin-based trafficking. PLoS Biol 13, e1002097.

Chang F, Martin SG (2009). Shaping fission yeast with microtubules. Cold Spring Harb Perspect Biol 1, a001347.

Chang F, Minc N (2014). Electrochemical control of cell and tissue polarity. Annu Rev Cell Dev Biol 30, 317–336.

Das A, Slaughter BD, Unruh JR, Bradford WD, Alexander R, Rubinstein B, Li R (2012). Flippase-mediated phospholipid asymmetry promotes fast Cdc42 recycling in dynamic maintenance of cell polarity. Nat Cell Biol 14, 304–310.

Das M, Wiley DJ, Chen X, Shah K, Verde F (2009). The conserved NDR kinase Orb6 controls polarized cell growth by spatial regulation of the small GTPase Cdc42. Curr Biol 19, 1314–1319.

Das M, Wiley DJ, Medina S, Vincent HA, Larrea M, Oriolo A, Verde F (2007). Regulation of cell diameter, For3p localization, and cell symmetry by fission yeast Rho-GAP Rga4p. Mol Biol Cell 18, 2090–2101.

Estravis M, Rincon SA, Santos B, Perez P (2011). Cdc42 regulates multiple membrane traffic events in fission yeast. Traffic 12, 1744–1758.
Fairn GD, Hermansson M, Somerharju P, Grinstein S (2011a). Phosphatidylserine is polarized and required for proper Cdc42 localization and for development of cell polarity. Nat Cell Biol 13, 1424–1430.
Fairn GD, Schieber NL, Ariotti N, Murphy S, Kuerschner L, Webb RI, Grinstein S, Parton RG (2011b). High-resolution mapping reveals topologically distinct cellular pools of phosphatidylserine. J Cell Biol 194, 257–275.
Feierbach B, Chang F (2001). Roles of the fission yeast formin for3p in cell polarity, actin cable formation and symmetric cell division. Curr Biol 11, 1656–1665.
Ghosh S, Xie WQ, Quest AF, Mabrouk GM, Strum JC, Bell RM (1994). The cysteine-rich region of raf-1 kinase contains zinc, translocates to liposomes, and is adjacent to a segment that binds GTP-ras. J Biol Chem 269, 10000–10007.
Gietz RD, Schiestl RH, Willems AR, Woods RA (1995). Studies on the transformation of intact yeast cells by the LiAc/SS-DNA/PEG procedure. Yeast 11, 355–360.
Haupt A, Campetelli A, Bonazzi D, Piel M, Chang F, Minc N (2014). Electrochemical regulation of budding yeast polarity. PLoS Biol 12, e1002029.
Heo WD, Inoue T, Park WS, Kim ML, Park BO, Wandless TJ, Meyer T (2006). PI(3,4,5)P3 and PI(4,5)P2 lipids target proteins with polybasic clusters to the plasma membrane. Science 314, 1458–1461.
Iwaki T, Tanaka N, Takagi H, Giga-Hama Y, Takegawa K (2004). Characterization of *end4*$^{+}$, a gene required for endocytosis in *Schizosaccharomyces pombe*. Yeast 21, 867–881.
Kay JG, Koivusalo M, Ma X, Wohland T, Grinstein S (2012). Phosphatidylserine dynamics in cellular membranes. Mol Biol Cell 23, 2198–2212.
Lee WL, Bezanilla M, Pollard TD (2000). Fission yeast myosin-I, Myo1p, stimulates actin assembly by Arp2/3 complex and shares functions with WASp. J Cell Biol 151, 789–800.
Li L, Shi X, Guo X, Li H, Xu C (2014). Ionic protein-lipid interaction at the plasma membrane: what can the charge do? Trends Biochem Sci 39, 130–140.
Maeda K, Anand K, Chiapparino A, Kumar A, Poletto M, Kaksonen M, Gavin AC (2013). Interactome map uncovers phosphatidylserine transport by oxysterol-binding proteins. Nature 501, 257–261.
Maekawa M, Fairn GD (2015). Complementary probes reveal that phosphatidylserine is required for the proper transbilayer distribution of cholesterol. J Cell Sci 128, 1422–1433.
Makushok T, Alves P, Huisman SM, Kijowski AR, Brunner D (2016). Sterol-rich membrane domains define fission yeast cell polarity. Cell 165, 1182–1196.
Martin SG, Rincon SA, Basu R, Perez P, Chang F (2007). Regulation of the formin for3p by cdc42p and bud6p. Mol Biol Cell 18, 4155–4167.
Martin SW, Konopka JB (2004). Lipid raft polarization contributes to hyphal growth in *Candida albicans*. Eukaryot Cell 3, 675–684.
Matsuo Y, Fisher E, Patton-Vogt J, Marcus S (2007). Functional characterization of the fission yeast phosphatidylserine synthase gene, pps1, reveals novel cellular functions for phosphatidylserine. Eukaryot Cell 6, 2092–2101.
Maundrell K (1993). Thiamine-repressible expression vectors pREP and pRIP for fission yeast. Gene 123, 127–130.
Nakano K, Arai R, Mabuchi I (1997). The small GTP-binding protein Rho1 is a multifunctional protein that regulates actin localization, cell polarity, and septum formation in the fission yeast *Schizosaccharomyces pombe*. Genes Cells 2, 679–694.
Nishizuka Y (1992). Intracellular signaling by hydrolysis of phospholipids and activation of protein kinase C. Science 258, 607–614.
Olivotto M, Arcangeli A, Carla M, Wanke E (1996). Electric fields at the plasma membrane level: a neglected element in the mechanisms of cell signalling. Bioessays 18, 495–504.
Perez P, Rincon SA (2010). Rho GTPases: regulation of cell polarity and growth in yeasts. Biochem J 426, 243–253.
Pike LJ, Han X, Gross RW (2005). Epidermal growth factor receptors are localized to lipid rafts that contain a balance of inner and outer leaflet lipids: a shotgun lipidomics study. J Biol Chem 280, 26796–26804.
Roy MO, Leventis R, Silvius JR (2000). Mutational and biochemical analysis of plasma membrane targeting mediated by the farnesylated, polybasic carboxy terminus of K-ras4B. Biochemistry 39, 8298–8307.
Sato M, Dhut S, Toda T (2005). New drug-resistant cassettes for gene disruption and epitope tagging in *Schizosaccharomyces pombe*. Yeast 22, 583–591.
Simons M *et al*. (2009). Electrochemical cues regulate assembly of the Frizzled/Dishevelled complex at the plasma membrane during planar epithelial polarization. Nat Cell Biol 11, 286–294.
Soto T, Villar-Tajadura MA, Madrid M, Vicente J, Gacto M, Perez P, Cansado J (2010). Rga4 modulates the activity of the fission yeast cell integrity MAPK pathway by acting as a Rho2 GTPase-activating protein. J Biol Chem 285, 11516–11525.
Spira F, Mueller NS, Beck G, von Olshausen P, Beig J, Wedlich-Soldner R (2012). Patchwork organization of the yeast plasma membrane into numerous coexisting domains. Nat Cell Biol 14, 640–648.
Takeda T, Chang F (2005). Role of fission yeast myosin I in organization of sterol-rich membrane domains. Curr Biol 15, 1331–1336.
Tatebe H, Nakano K, Maximo R, Shiozaki K (2008). Pom1 DYRK regulates localization of the Rga4 GAP to ensure bipolar activation of Cdc42 in fission yeast. Curr Biol 18, 322–330.
Vance JE (2008). Phosphatidylserine and phosphatidylethanolamine in mammalian cells: two metabolically related aminophospholipids. J Lipid Res 49, 1377–1387.
van Meer G, Voelker DR, Feigenson GW (2008). Membrane lipids: where they are and how they behave. Nat Rev Mol Cell Biol 9, 112–124.
Wachtler V, Rajagopalan S, Balasubramanian MK (2003). Sterol-rich plasma membrane domains in the fission yeast *Schizosaccharomyces pombe*. J Cell Sci 116, 867–874.
Wang H, Tang X, Liu J, Trautmann S, Balasundaram D, McCollum D, Balasubramanian MK (2002). The multiprotein exocyst complex is essential for cell separation in *Schizosaccharomyces pombe*. Mol Biol Cell 13, 515–529.
Win TZ, Gachet Y, Mulvihill DP, May KM, Hyams JS (2001). Two type V myosins with nonoverlapping functions in the fission yeast *Schizosaccharomyces pombe*: Myo52 is concerned with growth polarity and cytokinesis, Myo51 is a component of the cytokinetic actin ring. J Cell Sci 114, 69–79.
Yeung T, Gilbert GE, Shi J, Silvius J, Kapus A, Grinstein S (2008). Membrane phosphatidylserine regulates surface charge and protein localization. Science 319, 210–213.
Yeung T, Heit B, Dubuisson JF, Fairn GD, Chiu B, Inman R, Kapus A, Swanson M, Grinstein S (2009). Contribution of phosphatidylserine to membrane surface charge and protein targeting during phagosome maturation. J Cell Biol 185, 917–928.
Zhang Y, Sugiura R, Lu Y, Asami M, Maeda T, Itoh T, Takenawa T, Shuntoh H, Kuno T (2000). Phosphatidylinositol 4-phosphate 5-kinase Its3 and calcineurin Ppb1 coordinately regulate cytokinesis in fission yeast. J Biol Chem 275, 35600–35606.